AIAA JOURNAL
Vol. 37, No. 10, October 1999

Nonbaseband Residual Flexibility Method of Component Mode Synthesis for Proportionally Damped Systems

Jeffrey A. Morgan*
General Motors Corporation, Warren, Michigan 48090-9060
and
Christophe Pierre† and Gregory M. Hulbert‡
University of Michigan, Ann Arbor, Michigan 48109-2125

Several new component mode synthesis methods are presented for the dynamic analysis of proportionally damped systems in nonbaseband frequency regions of interest. The first method is based on the Craig–Bampton constraint modes approach (Craig, R. R., Jr., and Bampton, M. C. C., "Coupling of Substructures for Dynamic Analyses," *AIAA Journal*, Vol. 6, No. 7, 1968, pp. 1313–1319) but uses a modified dynamic transformation method that produces constraint modes at two frequencies, normally the upper and lower frequency limits of the region of interest. Then, a second method is presented that is similar to the first but uses a residual flexibility formulation. This second method is ideally suited for use with test-derived data and becomes the basis for a new nonbaseband experimentally based method. The procedure for implementing the experimentally based method is then presented. Finally, an analytical simulation is conducted using error-free data to demonstrate the new methods on a system of two coupled beams.

Nomenclature

$\bar{B}$	= undamped system matrix
C	= damping matrix
$c, \bar{c}$	= damping parameters in approximate residual functions
ei	= modulus of elasticity times bending moment of inertia
e^2	= squared error
$\boldsymbol{F}$	= force vector
H_{approx}	= frequency-response function calculated from component modes synthesis representation
H_{meas}	= measured frequency-response function
I	= identity matrix
K	= stiffness matrix
$k, \hat{k}, \bar{k}$	= stiffness parameters in approximate residual functions
M	= mass matrix
$m, \bar{m}$	= mass parameters in approximate residual functions
n	= number of measured frequencies
R	= residual matrix
$R^N_{\text{type I}}$	= type I residual function
$R^N_{\text{type II}}$	= type II residual function
$T^N, \bar{T}^N$	= transformation matrices
$\hat{T}^N$	= transformation matrix
$\boldsymbol{X}$	= response vector
x_i	= displacement of node i
Γ, Ψ	= partitioned transformation matrices
λ	= modal frequencies
ρa	= mass density times cross-sectional area
Υ, Ω	= partitioned transformation matrices
Φ	= modal vectors
ω	= frequency, rad/s
ω_1	= lower frequency limit, rad/s
ω_2	= upper frequency limit, rad/s

Subscripts

a	= active degrees of freedom (DOF)
cb	= Craig–Bampton type
cm	= constraint mode type
comp	= computational type
l	= lower modes
o	= omitted DOF
p, q, r	= intermediate DOF
rf	= residual flexibility type
s	= modal DOF
t, v	= intermediate DOF
u	= upper modes

Superscripts

C	= curvature type
F	= flexibility type
G, H	= auxiliary type
I	= inertance type
l	= lower modes
S	= slope type
u	= upper modes

I. Introduction

MOST existing methods of component modes synthesis (CMS) utilize static reduction; thus, they are inherently baseband methods applicable to frequency regions starting at 0 Hz and ending at a specified upper frequency limit. In many cases, however, the frequency region of interest may not be a baseband. This paper presents several new component mode synthesis methods applicable to proportionally damped systems and nonbaseband frequency regions of interest. Both analytical and experimentally based versions of the new methods are developed. The analytical versions are a nonbaseband constraint modes CMS method and a residual flexibility CMS method. The residual flexibility method is used as the basis for a new experimentally based method. The concept of computational modes is used in exactly the same manner as was done for the previously developed experimentally based baseband method.[1,2] Computational modes account for the residual effects of the omitted modes. For the nonbaseband case, two sets of computational modes are produced, which correspond to upper and lower computational modes. The upper computation modes are handled in the same manner as with the baseband method. The lower computational modes are handled similarly, except that the high-frequency behavior is preserved instead of the low-frequency behavior. Then, the matrices corresponding to the nonbaseband residual flexibility method are transformed to the Craig–Bampton[3] form using a two-stage transformation.

Received 12 August 1998; revision received 21 January 1999; accepted for publication 3 February 1999.

*Senior Project Engineer, Synthesis and Analysis Department, General Motors Powertrain Division, Mail Loc. 480-723-828, 30003 Van Dyke Avenue.

†Professor, Department of Mechanical Engineering and Applied Mechanics, 2204 G.G. Brown. Senior Member AIAA.

‡Associate Professor, Department of Mechanical Engineering and Applied Mechanics, 2250 G.G. Brown.

The major contribution of the new methods is that they allow accurate CMS models to be determined for specific frequency regions of interest, such as those used for noise control in vehicles. In this regard, they are optimal dynamic models because they require a minimum number of degrees of freedom (DOF). Both analytical and test-derived matrices can be determined. This allows the dynamic analysis of large systems to be performed using a mixture of both types of models. The test-derived models can also be directly compared to analytically derived models for the purpose of finite element analysis (FEA) model correlation and updating. FEA model verification is more easily conducted, and the inclusion of damping into analytical models, as well as insights into the physical damping mechanisms of actual systems, is facilitated.

This paper is organized as follows. The new nonbaseband constraint modes CMS method is presented in Sec. II. Then, the new nonbaseband residual flexibility method is presented in Sec. III. In Sec. IV, the procedure for transforming the residual flexibility matrices to the Craig–Bampton form is shown. Then, the procedure for implementing the experimentally based method is presented in Sec. V. In Sec. VI, an analytical simulation is conducted using error-free data to demonstrate the new methods on a system of two coupled beams. Conclusions are drawn in Sec. VII.

II. Nonbaseband Constraint Modes CMS Method

The new nonbaseband constraint modes CMS method is developed as follows. Consider a substructure governed by the matrix equation of motion

$$M\ddot{\boldsymbol{X}} + C\dot{\boldsymbol{X}} + K\boldsymbol{X} = \boldsymbol{F} \tag{1}$$

where K, M, and C are the substructure's global stiffness, mass, and damping matrices and $\boldsymbol{X}$ and $\boldsymbol{F}$ are the displacement and external loading vectors, respectively. It is assumed that the substructure representation is proportionally damped so that the vibrational modes corresponding to Eq. (1) are the normal modes of vibration of the undamped system. For dynamic analysis in a nonbaseband region, the matrices in Eq. (1) can be transformed to a reduced set of DOF while retaining a high degree of accuracy in the frequency region of interest. The reduced DOF set is selected using the same procedure as for the Craig–Bampton method[3] except that constraint modes are calculated at the upper and lower frequency limits of the nonbaseband region instead of at zero frequency. To do this, the displacement DOF are selected as either active or omitted. An active DOF is one that is retained directly in the reduced DOF set. An omitted DOF is one that is not retained. Active DOF should include all displacement DOF where nonzero external loading is present. For substructure coupling analysis, these are all of the coupling DOF between substructures and any noncoupling DOF where external loading is applied. The displacement vector $\boldsymbol{X}$ is then partitioned as

$$\boldsymbol{X} = \begin{bmatrix} \boldsymbol{X}_o \\ \boldsymbol{X}_a \end{bmatrix} \tag{2}$$

where the subscripts a and o refer to the active and omitted DOF, respectively. The matrices K, M, and C and the vector $\boldsymbol{F}$ are partitioned likewise. Constraint modes then can be calculated at any particular frequency using the procedure presented by Shyu et al.[4] This is done by considering the undamped equation of motion

$$\bar{B}\begin{bmatrix} \boldsymbol{X}_o \\ \boldsymbol{X}_a \end{bmatrix} = \begin{bmatrix} \bar{B}_{oo} & \bar{B}_{oa} \\ [\bar{B}_{oa}]^T & \bar{B}_{aa} \end{bmatrix}\begin{bmatrix} \boldsymbol{X}_o \\ \boldsymbol{X}_a \end{bmatrix} = \begin{bmatrix} \boldsymbol{0} \\ \boldsymbol{F}_a \end{bmatrix} \tag{3}$$

where $\bar{B} = K - \omega^2 M$ is the undamped global system matrix corresponding to Eq. (1). Solving the first matrix equation in Eq. (3) for $\boldsymbol{X}_o$ in terms of $\boldsymbol{X}_a$, with $\omega = \omega_1$, gives

$$\boldsymbol{X} = \begin{bmatrix} \Psi_{oa}(\omega_1) \\ I_{aa} \end{bmatrix}\boldsymbol{X}_a = \bar{\Psi}(\omega_1)\boldsymbol{X}_a \tag{4}$$

where $\Psi_{oa}(\omega_1) = -[\bar{B}_{oo}(\omega_1)]^{-1}\bar{B}_{oa}(\omega_1)$. $\bar{\Psi}(\omega_1)$ is the matrix of constraint modes at frequency ω_1. Because damping is neglected, the constraint modes are real valued.

For the new nonbaseband method, two sets of constraint modes are determined. The first set is calculated at the lower frequency limit of the nonbaseband region ω_1. The second set is calculated at the upper frequency limit of the nonbaseband region ω_2. To achieve an accurate CMS representation, additional reduced DOF are usually needed. These additional DOF correspond to component normal modes of the substructure. Component normal modes are determined by solving the eigenvalue problem obtained from Eq. (1) by setting $\boldsymbol{F} = \boldsymbol{0}$ and $C = 0$ with free boundary conditions applied to the active DOF. Only the modes that occur in the frequency region of interest are calculated and included as component modes. These modal vectors are then partitioned with respect to the active and omitted DOF:

$$\Phi = \begin{bmatrix} \Phi_{os} \\ \Phi_{as} \end{bmatrix} \tag{5}$$

where the subscript s refers to the number of modal vectors included. The new method's transformation matrix is then determined from the two sets of constraint modes and the component modes:

$$\begin{bmatrix} \boldsymbol{X}_o \\ \boldsymbol{X}_a \end{bmatrix} = \begin{bmatrix} \Psi_{oa}(\omega_1) & \Omega_{oa} & \Upsilon_{os} \\ I_{aa} & 0_{aa} & 0_{as} \end{bmatrix}\begin{bmatrix} \boldsymbol{X}_a \\ \boldsymbol{X}_q \\ \boldsymbol{X}_s \end{bmatrix} = T_{\text{cm}}^N \begin{bmatrix} \boldsymbol{X}_a \\ \boldsymbol{X}_q \\ \boldsymbol{X}_s \end{bmatrix} \tag{6}$$

where $\boldsymbol{X}_q$ and $\boldsymbol{X}_a$ have the same dimensions, $\Omega_{oa} = \Psi_{oa}(\omega_2) - \Psi_{oa}(\omega_1)$ and $\Upsilon_{os} = \Phi_{os} - \Psi_{oa}(\omega_1)\Phi_{as}$. The matrix T_{cm}^N is defined as the nonbaseband constraint modes transformation matrix. The reduced stiffness, mass, and damping matrices are determined by transforming the substructure's global matrices using T_{cm}^N, which yields

$$K_{\text{cm}}^N = \left[T_{\text{cm}}^N\right]^T K T_{\text{cm}}^N \tag{7}$$

$$M_{\text{cm}}^N = \left[T_{\text{cm}}^N\right]^T M T_{\text{cm}}^N \tag{8}$$

$$C_{\text{cm}}^N = \left[T_{\text{cm}}^N\right]^T C T_{\text{cm}}^N \tag{9}$$

Dynamic analyses can then be conducted. The results are determined using the reduced DOF representation and are transformed back to the original set using Eq. (6).

The nonbaseband constraint modes CMS method can also be expressed as a modal expansion. This is done by calculating the natural frequencies and modal vectors corresponding to Eqs. (7–9) and by representing them as a modal expansion. The modes involved in the modal expansion include the original component modes and an additional set of computational modes. The computational modes, in general, do not correspond to any of the original vibrational modes of the substructure. They occur outside the frequency region of interest and account for the residual effects of the omitted structural modes. In this case, $2a$ computational modes are produced, which correspond to upper and lower computational modes. The upper computational modes occur above the frequency region of interest and account for the residual effects of the high-frequency omitted modes. The lower computational modes occur below the frequency region of interest and account for the residual effects of the low-frequency omitted modes. This observation allows both a nonbaseband residual flexibility method and a nonbaseband experimentally based CMS method to be developed, as presented in the following section.

III. Nonbaseband Residual Flexibility CMS Method

The new nonbaseband residual flexibility method is developed based on the nonbaseband constraint modes CMS method. The method utilizes the same selection criteria for the active and omitted DOF and for the component modes as for the nonbaseband constraint modes CMS method. Additionally, it is assumed that of the $2a$ computational modes, there are a that occur below the frequency region of interest and a that occur above. This allows the lower and upper computational modes to be determined independently.

The new nonbaseband residual flexibility formulation can be developed as follows. Consider the complete set of modal frequencies and modal vectors determined by solving the eigenvalue problem corresponding to Eq. (1). The modal frequencies and modal vectors

are partitioned with respect to the included modes, omitted low-frequency modes, and omitted high-frequency modes:

$$\lambda = \begin{bmatrix} \lambda_{ll} & 0_{ls} & 0_{lu} \\ 0_{sl} & \lambda_{ss} & 0_{su} \\ 0_{ul} & 0_{us} & \lambda_{uu} \end{bmatrix} \tag{10}$$

$$\Phi = \begin{bmatrix} \Phi_{ol} & \Phi_{os} & \Phi_{ou} \\ \Phi_{al} & \Phi_{as} & \Phi_{au} \end{bmatrix} \tag{11}$$

where subscript s refers to the number of included modal vectors. Subscripts l and u refer to the number of omitted low-frequency and high-frequency modal vectors, respectively. With the modal vectors scaled to unity modal mass, the residual flexibility matrix corresponding to the omitted high-frequency modes is

$$R^F = \begin{bmatrix} \Phi_{ou} \\ \Phi_{au} \end{bmatrix} \lambda_{uu}^{-1} \begin{bmatrix} \Phi_{ou}^T & \Phi_{au}^T \end{bmatrix} = \begin{bmatrix} R_{oo}^F & R_{oa}^F \\ \left[R_{oa}^F\right]^T & R_{aa}^F \end{bmatrix} \tag{12}$$

Similarly, the residual inertance of the omitted low-frequency modes is

$$R^I = \begin{bmatrix} \Phi_{ol} \\ \Phi_{al} \end{bmatrix} \begin{bmatrix} \Phi_{ol}^T & \Phi_{al}^T \end{bmatrix} = \begin{bmatrix} R_{oo}^I & R_{oa}^I \\ \left[R_{oa}^I\right]^T & R_{aa}^I \end{bmatrix} \tag{13}$$

The residual effects of the omitted high-frequency modes are compensated for by the upper computational modes. These modes produce primarily stiffness effects in the frequency region of interest. Therefore, the transformation matrix is determined using the residual flexibility matrix. The low-frequency stiffness behavior for zero forces on the omitted DOF is

$$\begin{bmatrix} \boldsymbol{X}_o \\ \boldsymbol{X}_a \end{bmatrix} = \begin{bmatrix} R_{oo}^F & R_{oa}^F \\ \left[R_{oa}^F\right]^T & R_{aa}^F \end{bmatrix} \begin{bmatrix} \boldsymbol{0} \\ \boldsymbol{F}_a \end{bmatrix} \tag{14}$$

Solving the matrix equations in Eq. (14) for $\boldsymbol{X}_o$ in terms of $\boldsymbol{X}_a$ allows the low-frequency response vector $\boldsymbol{X}$ to be expressed as

$$\boldsymbol{X} = \begin{bmatrix} \Gamma_{oa}^u \\ I_{aa} \end{bmatrix} \boldsymbol{X}_a \tag{15}$$

where $\Gamma_{oa}^u = R_{oa}^F \left[R_{aa}^F\right]^{-1}$. Equation (15) is the same constraint relation used in previously developed baseband residual flexibility CMS methods (see Kammer and Baker[5] for an overview of these methods; also see Refs. 6 and 7 for other residual flexibility approaches).

The residual effects of the omitted low-frequency modes are compensated for by the lower computational modes. The omitted low-frequency modes produce primarily mass effects in the frequency region of interest. Therefore, the transformation matrix is determined using the residual inertance matrix. The high-frequency mass behavior for zero forces on the omitted DOF is

$$\begin{bmatrix} \boldsymbol{X}_o \\ \boldsymbol{X}_a \end{bmatrix} = \frac{-1}{\omega^2} \begin{bmatrix} R_{oo}^I & R_{oa}^I \\ \left[R_{oa}^I\right]^T & R_{aa}^I \end{bmatrix} \begin{bmatrix} \boldsymbol{0} \\ \boldsymbol{F}_a \end{bmatrix} \tag{16}$$

Solving the matrix equations in Eq. (16) for $\boldsymbol{X}_o$ in terms of $\boldsymbol{X}_a$ allows the high-frequency response vector $\boldsymbol{X}$ to be expressed as

$$\boldsymbol{X} = \begin{bmatrix} \Gamma_{oa}^l \\ I_{aa} \end{bmatrix} \boldsymbol{X}_a \tag{17}$$

where $\Gamma_{oa}^l = R_{oa}^I \left[R_{aa}^I\right]^{-1}$. The new nonbaseband residual flexibility transformation matrix is then defined as

$$\begin{bmatrix} \boldsymbol{X}_o \\ \boldsymbol{X}_a \end{bmatrix} = \begin{bmatrix} \Gamma_{oa}^u & \Gamma_{oa}^l & \Phi_{os} \\ I_{aa} & I_{aa} & \Phi_{as} \end{bmatrix} \begin{bmatrix} \boldsymbol{X}_r \\ \boldsymbol{X}_q \\ \boldsymbol{X}_s \end{bmatrix} = T_{\text{rf}}^N \begin{bmatrix} \boldsymbol{X}_r \\ \boldsymbol{X}_q \\ \boldsymbol{X}_s \end{bmatrix} \tag{18}$$

where $\boldsymbol{X}_r$ and $\boldsymbol{X}_q$ have the same dimensions as $\boldsymbol{X}_a$. The reduced stiffness, mass, and damping matrices are calculated as shown in Eqs. (7–9) using T_{rf}^N, which yields

$$K_{\text{rf}}^N = \begin{bmatrix} K_{\text{comp}}^u & 0_{aa} & 0_{as} \\ 0_{aa} & K_{\text{comp}}^l & 0_{as} \\ 0_{sa} & 0_{sa} & K_{ss} \end{bmatrix} \tag{19}$$

$$M_{\text{rf}}^N = \begin{bmatrix} M_{\text{comp}}^u & 0_{aa} & 0_{as} \\ 0_{aa} & M_{\text{comp}}^l & 0_{as} \\ 0_{sa} & 0_{sa} & M_{ss} \end{bmatrix} \tag{20}$$

$$C_{\text{rf}}^N = \begin{bmatrix} C_{\text{comp}}^u & 0_{aa} & 0_{as} \\ 0_{aa} & C_{\text{comp}}^l & 0_{as} \\ 0_{sa} & 0_{sa} & C_{ss} \end{bmatrix} \tag{21}$$

IV. Transformation to the Craig–Bampton Form

The newly defined nonbaseband residual flexibility method produces reduced matrices that are not in a convenient form because the active DOF are not retained in the reduced DOF set. To remedy this, the same two-stage transformation procedure developed in Ref. 1 is used. The resulting matrices will then have the same form as the Craig–Bampton method but are valid for the nonbaseband regions. The first transformation is from the reduced DOF in Eq. (18) using

$$\begin{bmatrix} \boldsymbol{X}_r \\ \boldsymbol{X}_q \\ \boldsymbol{X}_s \end{bmatrix} = \begin{bmatrix} I_{aa} & -I_{aa} & -\Phi_{as} \\ 0_{aa} & I_{aa} & 0_{as} \\ 0_{as} & 0_{as} & I_{ss} \end{bmatrix} \begin{bmatrix} \boldsymbol{X}_a \\ \boldsymbol{X}_q \\ \boldsymbol{X}_s \end{bmatrix} = \hat{T}^N \begin{bmatrix} \boldsymbol{X}_a \\ \boldsymbol{X}_q \\ \boldsymbol{X}_s \end{bmatrix} \tag{22}$$

Transforming Eqs. (19–21) gives

$$\hat{K} = \begin{bmatrix} K_{\text{comp}}^u & \begin{bmatrix} -K_{\text{comp}}^u & -K_{\text{comp}}^u \Phi_{as} \end{bmatrix} \\ \begin{bmatrix} -K_{\text{comp}}^u \\ -\Phi_{as}^T K_{\text{comp}}^u \end{bmatrix} & \begin{bmatrix} \left(K_{\text{comp}}^u + K_{\text{comp}}^l\right) & K_{\text{comp}}^u \Phi_{as} \\ \Phi_{as}^T K_{\text{comp}}^u & \left(\Phi_{as}^T K_{\text{comp}}^u \Phi_{as} + K_{ss}\right) \end{bmatrix} \end{bmatrix} = \begin{bmatrix} K_{\text{comp}}^u & \tilde{K} \\ \tilde{K}^T & \bar{K} \end{bmatrix} \tag{23}$$

$$\hat{M} = \begin{bmatrix} M_{\text{comp}}^u & \begin{bmatrix} -M_{\text{comp}}^u & -M_{\text{comp}}^u \Phi_{as} \end{bmatrix} \\ \begin{bmatrix} -M_{\text{comp}}^u \\ -\Phi_{as}^T M_{\text{comp}}^u \end{bmatrix} & \begin{bmatrix} \left(M_{\text{comp}}^u + M_{\text{comp}}^l\right) & M_{\text{comp}}^u \Phi_{as} \\ \Phi_{as}^T M_{\text{comp}}^u & \left(\Phi_{as}^T M_{\text{comp}}^u \Phi_{as} + M_{ss}\right) \end{bmatrix} \end{bmatrix} = \begin{bmatrix} M_{\text{comp}}^u & \tilde{M} \\ \tilde{M}^T & \bar{M} \end{bmatrix} \tag{24}$$

$$\hat{C} = \begin{bmatrix} C_{\text{comp}}^u & \begin{bmatrix} -C_{\text{comp}}^u & -C_{\text{comp}}^u \Phi_{as} \end{bmatrix} \\ \begin{bmatrix} -C_{\text{comp}}^u \\ -\Phi_{as}^T C_{\text{comp}}^u \end{bmatrix} & \begin{bmatrix} \left(C_{\text{comp}}^u + C_{\text{comp}}^l\right) & C_{\text{comp}}^u \Phi_{as} \\ \Phi_{as}^T C_{\text{comp}}^u & \left(\Phi_{as}^T C_{\text{comp}}^u \Phi_{as} + C_{ss}\right) \end{bmatrix} \end{bmatrix} = \begin{bmatrix} C_{\text{comp}}^u & \tilde{C} \\ \tilde{C}^T & \bar{C} \end{bmatrix} \tag{25}$$

where the reduced matrices are partitioned using

$$\boldsymbol{X}_v = \begin{bmatrix} \boldsymbol{X}_q \\ \boldsymbol{X}_s \end{bmatrix} \tag{26}$$

The second transformation is from the reduced DOF in Eq. (22) using

$$\begin{bmatrix} \boldsymbol{X}_a \\ \boldsymbol{X}_v \end{bmatrix} = \begin{bmatrix} I_{aa} & 0_{av} \\ Z_{va} & U_{vv} \end{bmatrix} \begin{bmatrix} \boldsymbol{X}_a \\ \boldsymbol{X}_t \end{bmatrix} = \bar{T}^N \begin{bmatrix} \boldsymbol{X}_a \\ \boldsymbol{X}_t \end{bmatrix} \tag{27}$$

where $\boldsymbol{X}_t$ has the same dimensions as $\boldsymbol{X}_v$ and where $Z_{va} = -\bar{K}^{-1} \tilde{K}^T$ is determined by static reduction of Eq. (23) and the matrix U_{vv} is determined from the eigenvectors of

$$\bar{M}\ddot{\boldsymbol{X}}_v + \bar{C}\dot{\boldsymbol{X}}_v \bar{K}\boldsymbol{X}_v = \boldsymbol{0} \tag{28}$$

The transformation matrix from the new nonbaseband residual flexibility formulation to the Craig–Bampton form is then

$$T^N_{\text{cb}} = T^N_{\text{rf}} T^N \tag{29}$$

where $T^N = \hat{T}^N \bar{T}^N$.

V. Experimentally Based Nonbaseband CMS Method

The new experimentally based nonbaseband CMS method is developed based on the nonbaseband residual flexibility method. The procedure is analogous to that developed for baseband regions in Refs. 1 and 2. First, the Maclaurin series expansion coefficients corresponding to the residual effects of the omitted modes are determined using approximate residual functions and an optimization procedure. Second, the upper and lower computational modes are calculated by equating the Maclaurin series expansion coefficients corresponding to the omitted modes to that of the computational modes. Third, model refinement is conducted to minimize errors in the representation caused by measurement noise and the optimization procedure.

A. Estimation of the Maclaurin Series Expansion Coefficients Using Approximate Residual Functions

The estimation of the Maclaurin series expansion coefficients is done using approximate residual functions that are designed to produce stiffness, mass, and damping effects in the frequency region of interest in exactly the same manner as for the omitted modes. Two types of approximate residual functions are defined to represent the two types of exact residual functions that may occur. Then the parameters corresponding to the approximate residual functions are determined using optimization.

Two approximate residual functions are defined based on the presence or absence of an antiresonance in the frequency region of interest. A type I residual is defined such that no antiresonance occurs in the frequency region of interest, and a type II residual is defined such that an antiresonance does occur:

$$R^N_{\text{type I}} = \frac{\text{sgn}(k)}{(\hat{k} - m\omega^2) + ic\omega} - \frac{\text{sgn}(k)}{(\bar{k} - \bar{m}\omega^2) + i\bar{c}\omega} \tag{30}$$

$$R^N_{\text{type II}} = \frac{\text{sgn}(k)}{(\hat{k} - m\omega^2) + ic\omega} + \frac{\text{sgn}(k)}{(\bar{k} - \bar{m}\omega^2) + i\bar{c}\omega} \tag{31}$$

where $\hat{k} = |k|$ and $m, c, \bar{k}, \bar{m}$, and $\bar{c} \geq 0$. These approximate residual functions are the addition or subtraction of two single-degree-of-freedom (SDOF) oscillators, with one occurring below the frequency region of interest and one above, as shown in Fig. 1. Each exact residual function is characterized as either type I or type II, and the corresponding approximate residual function is used during optimization. In either case, there are six independent optimization parameters. The parameter k corresponds to the inverse of the residual flexibility of the omitted high-frequency modes. The parameter $\bar{m}$ corresponds to the absolute value of the inverse of the residual inertance of the omitted low-frequency modes. These parameters are usually estimated in the structural modes curve-fitting process. The remaining parameters are determined using an optimization routine that minimizes the squared error between the measured frequency-response functions and the approximate representations in log-magnitude format as

$$e^2 = \frac{100}{n} \sum_{\omega=\omega_1}^{\omega_2} \left(\frac{\log|H_{\text{meas}}| - \log|H_{\text{approx}}|}{\log|H_{\text{meas}}|} \right)^2 \% \tag{32}$$

where n is the number of measured frequencies in the optimization region and provided $\log|H_{\text{meas}}| \neq 0$. Generally, the squared error function will not be sufficiently smooth to use gradient-based optimization methods. Furthermore, local optima may occur; therefore, either global search methods or a direct mapping of the search space should be conducted. This is feasible because only a small number of variables are to be optimized concurrently, and the search space can be narrowly defined based on the measured residual function.

Table 1 Maclaurin series expansion coefficients for the approximate residual functions

Approximate residual	$R^N_{\text{type I}}$	$R^N_{\text{type II}}$
R^F_{jl}	$1/k$	$1/k$
R^S_{jl}	$-\text{sgn}(k)(c/\hat{k}^2)$	$-\text{sgn}(k)(c/\hat{k}^2)$
R^C_{jl}	$-\text{sgn}(k)[-(m/\hat{k}^2) + (c^2/\hat{k}^3)]$	$-\text{sgn}(k)[-(m/\hat{k}^2) + (c^2/\hat{k}^3)]$
R^I_{jl}	$-\text{sgn}(k)(1/\bar{m})$	$\text{sgn}(k)(1/\bar{m})$
R^G_{jl}	$\text{sgn}(k)(\bar{c}/\bar{m}^2)$	$-\text{sgn}(k)(\bar{c}/\bar{m}^2)$
R^H_{jl}	$-\text{sgn}(k)[-(\bar{k}/\bar{m}^2) + (\bar{c}^2/\bar{m}^3)]$	$\text{sgn}(k)[-(\bar{k}/\bar{m}^2) + (\bar{c}^2/\bar{m}^3)]$

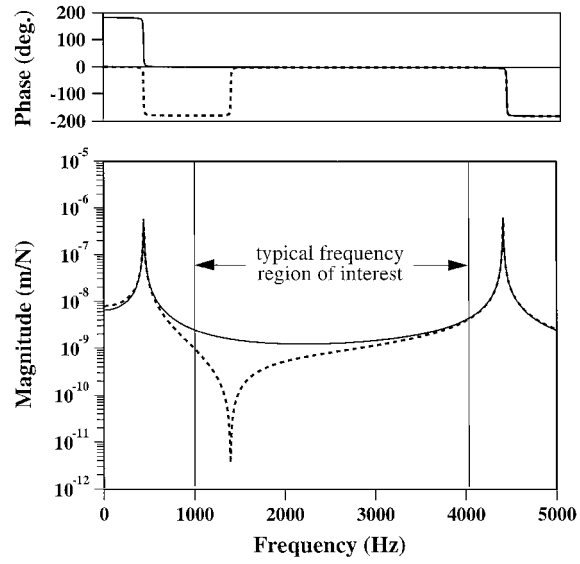

Fig. 1 Frequency-response functions for $R^N_{\text{type I}}$ (——) and $R^N_{\text{type II}}$ (- - - -) with $k = \hat{k} = 1.4 \times 10^9$ N/m, $m = 1.82$ kg, $c = 55.9$ Ns/m, $\bar{k} = 1.4 \times 10^8$ N/m, $\bar{m} = 18.2$ kg, and $\bar{c} = 559.0$ Ns/m.

If the system is lightly damped, the parameters $\hat{k}, m, \bar{k}$, and $\bar{m}$ are relatively uncoupled with respect to c and $\bar{c}$ and can be determined independently. This further reduces the number of optimization variables needed to be determined concurrently.

The Maclaurin series expansion coefficients are determined by considering each of the SDOF systems constituting the approximate residual functions separately. The SDOF system corresponding to the high-frequency mode is used to calculate the upper computational modes. The SDOF system corresponding to the low-frequency mode is used to calculate the lower computational modes. The values of the Maclaurin series expansion coefficients are determined directly from the optimized parameters as shown in Table 1.

B. Calculation of the Computational Modes

The high-frequency computational modes are estimated by requiring the second-order Maclaurin series expansion of the high-frequency computational modes be equal to that of the omitted high-frequency modes, which is the same method Rubin used in his procedure.[8] The second-order Maclaurin series expansion coefficients corresponding to the active DOF are

$$R_{aa} \cong R^F_{aa} + iR^S_{aa}\omega + R^C_{aa}\omega^2 \tag{33}$$

where R_{aa} is the residual function matrix corresponding to the omitted high-frequency modes and R^F_{aa}, R^S_{aa}, and R^C_{aa} are the respective residual flexibility, residual slope, and residual curvature matrices. Only the second-order Maclaurin series expansion coefficients corresponding to the active DOF are made equal (the coefficients corresponding to the omitted DOF will not, in general, be equal). This is done by requiring that

$$R^F_{aa} + iR^S_{aa}\omega + R^C_{aa}\omega^2 = H^u_{\text{comp}}\big|_{\omega=0} + \left.\frac{\mathrm{d}H^u_{\text{comp}}}{\mathrm{d}\omega}\right|_{\omega=0}\omega + \frac{1}{2}\left.\frac{\mathrm{d}^2H^u_{\text{comp}}}{\mathrm{d}\omega^2}\right|_{\omega=0}\omega^2 \tag{34}$$

where $H^u_{\text{comp}} = (K^u_{\text{comp}} + iC^u_{\text{comp}}\omega - M^u_{\text{comp}}\omega^2)^{-1}$ is the frequency-response function matrix with K^u_{comp}, M^u_{comp}, and C^u_{comp} being the stiffness, mass, and damping matrices, respectively, corresponding to the high-frequency computational modes. Thus,

$$K^u_{\text{comp}} = \left[R^F_{aa}\right]^{-1} \tag{35}$$

$$M^u_{\text{comp}} = \left[R^F_{aa}\right]^{-1}\left(R^C_{aa} + R^S_{aa}\left[R^F_{aa}\right]^{-1}R^S_{aa}\right)\left[R^F_{aa}\right]^{-1} \tag{36}$$

$$C^u_{\text{comp}} = -\left[R^F_{aa}\right]^{-1}R^S_{aa}\left[R^F_{aa}\right]^{-1} \tag{37}$$

The low-frequency computational modes are estimated as follows. The residual effects of the low-frequency omitted modes are primarily high-frequency mass effects. The high-frequency behavior corresponding the active DOF can be expressed as

$$R_{aa} \cong -R^I_{aa}(1/\omega^2) + iR^G_{aa}(1/\omega^3) + R^H_{aa}(1/\omega^4) \tag{38}$$

where R^I is the residual inertance and R^G and R^H are defined as shown in Table 1. Equation (38) is the same as a Maclaurin series with $s = 1/\omega$ as the expansion function and is evaluated as ω approaches infinity ($s = 0$). The terms proportional to 1 and s can be shown to be zero. Therefore, the high-frequency behavior of the low-frequency computational modes can be made equal to that of the omitted low-frequency modes by requiring that

$$-R^I_{aa}s^2 + iR^G_{aa}s^3 + R^H_{aa}s^4 = \left.\frac{1}{2}\frac{\mathrm{d}^2H^l_{\text{comp}}}{\mathrm{d}s^2}\right|_{s=0}s^2 + \left.\frac{1}{6}\frac{\mathrm{d}^3H^l_{\text{comp}}}{\mathrm{d}s^3}\right|_{s=0}s^3 + \left.\frac{1}{24}\frac{\mathrm{d}^4H^l_{\text{comp}}}{\mathrm{d}s^4}\right|_{s=0}s^4 \tag{39}$$

where $H^l_{\text{comp}} = (K^l_{\text{comp}} + iC^l_{\text{comp}}s^{-1} - M^l_{\text{comp}}s^{-2})^{-1}$ is the frequency-response function matrix with K^l_{comp}, M^l_{comp}, and C^l_{comp} being the stiffness, mass, and damping matrices, respectively, corresponding to the low-frequency computational modes. Solving in terms of R^I_{aa}, R^G_{aa}, and R^H_{aa} gives

$$K^l_{\text{comp}} = \left[R^I_{aa}\right]^{-1}\left(R^G_{aa}\left[R^I_{aa}\right]^{-1}R^G_{aa} - R^H_{aa}\right)\left[R^I_{aa}\right]^{-1} \tag{40}$$

$$M^l_{\text{comp}} = \left[R^I_{aa}\right]^{-1} \tag{41}$$

$$C^l_{\text{comp}} = -\left[R^I_{aa}\right]^{-1}R^G_{aa}\left[R^I_{aa}\right]^{-1} \tag{42}$$

provided R^I_{aa} is nonsingular. If R^I_{aa} is singular, then there are fewer omitted low-frequency modes than there are active DOF. In this case, the number of lower computational modes must be reduced to that of the rank of R^I_{aa}.

C. Model Refinement

Model refinement is usually needed because of errors in the estimated Maclaurin series expansion coefficients. First, errors may cause some of the frequencies corresponding to the computational modes to occur in the frequency region of interest. Because all upper computational modes should occur above the frequency region of interest, any that do not can be included using only static effects, i.e., set the modal mass and damping corresponding to these modes to zero. Similarly, any lower computational modes that occur in the frequency region of interest can be included using only inertia effects, i.e., set the modal stiffness and damping corresponding to these modes to zero. Second, the damping calculated for the computational modes generally will be nonproportional, even for proportionally damped systems. This is caused by the optimization process and measurement errors. In this case, complex computational modes can be used; however, the resulting formulation is considerably more complicated. An alternative is to use approximate normal modes by using the undamped eigenvectors to transform the damping matrix and then to neglect the off-diagonal terms. Third, once a corrected model is determined, stiffness, mass, and damping updating may be performed to further improve the representation. A simple method is proportional updating, where the matrices corresponding to the upper and lower computational modes are multiplied by scalar factors determined by minimizing the squared error between the measured frequency-response functions and the approximate representations using Eq. (32). For the upper computational modes, the mass matrix is usually selected for updating because the low-frequency mass effects are more difficult to estimate accurately in this case. For the lower computational modes, the stiffness matrix is usually selected for updating because the high-frequency stiffness effects are more difficult to estimate accurately in this case. Damping updating may be done at the modal level using a number of the computational modes nearest the frequency region of interest.

VI. Example Problem: Two Coupled Beams

A system of two coupled Bernoulli–Euler beams undergoing transverse vibrations, shown in Fig. 2, is analyzed to illustrate the nonbaseband methods. Calculated (error-free) frequency-response

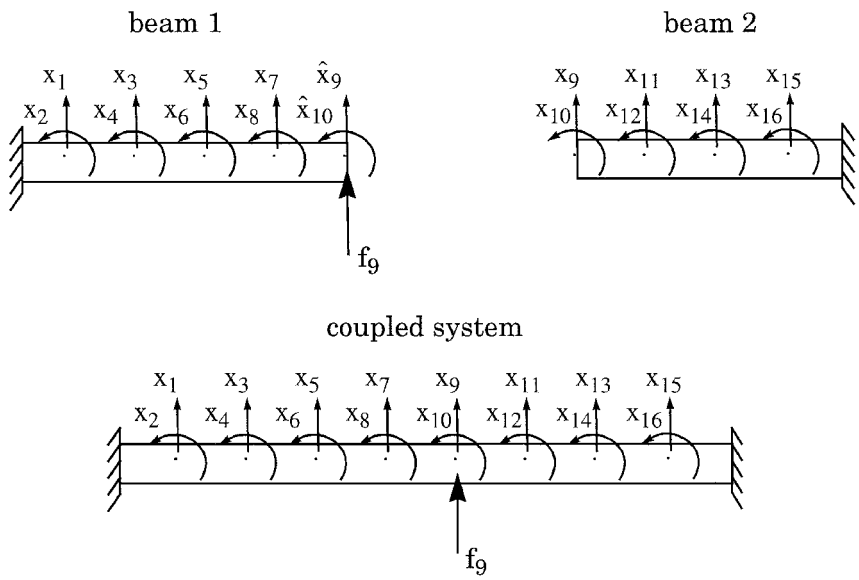

Fig. 2 System of two coupled beams.

functions are used, and damping is neglected. The length of beam 1 is 1.0 m, and the length of beam 2 is 0.8 m. The distance between DOF pairs for both beams is 0.2 m. Both beams are characterized by the mass density times area parameter, $\rho a = 100.0$ kg/m, and the elastic modulus times bending moment of inertia parameter, $ei = 2.0 \times 10^6$ Nm. The frequency region from 1000 to 4000 Hz is selected as the region of interest. The beams are directly coupled in the translational and rotational DOF at their connection interface: $\hat{x}_9 = x_9$ and $\hat{x}_{10} = x_{10}$. This results in the coupled system corresponding to a simple fixed–fixed beam. The excitation f_9 indicates the driving point location for the calculation of the coupled system's frequency-response functions, which is used to evaluate the accuracy of the methods.

The system of coupled beams is approximated by discretizing the beams at the locations shown in Fig. 2, using Hermite cubic shape functions, consistent mass matrices, and zero damping.[9] The exact solution of the discretized system is determined using modal analysis. The nonbaseband CMS methods will be conducted using reduced representations of beam 2. The results will be compared to the exact solution of the discretized system.

A. Nonbaseband Constraint Modes CMS Method

The system of two coupled beams was first analyzed using the nonbaseband constraint modes CMS method presented in Sec. II. Displacements x_9 and x_{10} were selected as the active DOF with the remaining displacements x_{11}–x_{16} as the omitted DOF. The constraint modes were calculated at frequencies $\omega_1 = 1000(2\pi)$ rad/s and $\omega_2 = 4000(2\pi)$ rad/s, which correspond to the lower and upper bounds of the frequency region of interest. Free boundary conditions were applied to the active DOF for the calculation of the vibrational modes as required. One vibrational mode occurred in the frequency region of interest and was included in the CMS representation. The transformation matrix was calculated from Eq. (6), and the reduced substructure matrices were determined. This results in a five-DOF representation for beam 2. The reduced matrices were assembled into the global system matrices. Then the eigenvalues and eigenvectors of these matrices were determined. The predicted driving point frequency-response function at point 9 and the exact solution are shown in Fig. 3. The coupled results using the nonbaseband constraints modes CMS method are seen to be virtually exact in the frequency region of interest.

B. Nonbaseband Residual Flexibility CMS Method

The nonbaseband residual flexibility CMS method was conducted on the system of two coupled beams. All of the vibrational modes of beam 2 were calculated using free boundary conditions applied to the active DOF. Then, the modal frequencies and modal vectors were partitioned as shown in Eqs. (10) and (11). This results in two low-frequency omitted modes, five high-frequency omitted modes, and one mode occurring in the frequency region of interest. The residual flexibility of the high-frequency omitted modes and the residual inertance of the low-frequency omitted modes are calculated from Eqs. (12) and (13). The transformation matrix is determined from Eq. (18). The reduced substructure matrices are determined and then transformed to the Craig–Bampton form using the two-stage transformation. These matrices are assembled into global matrices, and the eigenvalues and eigenvectors are determined. The predicted driving point frequency-response function at point 9 and the exact solution are shown in Fig. 4. The coupled results in this case are almost exact, except for the frequency of the fourth mode, which is predicted 2% high (4019 vs 3950 Hz).

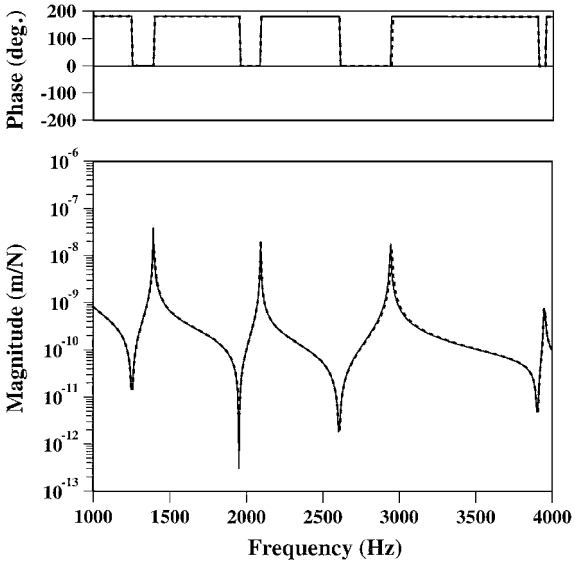

Fig. 3 Driving point frequency-response function at point 9 for the exact solution of the discretized system (——) and the nonbaseband analytical CMS constraint modes method (- - - -).

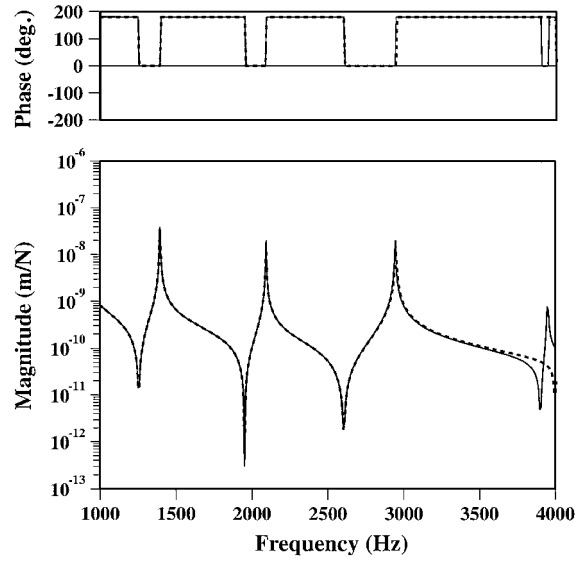

Fig. 4 Driving point frequency-response function at point 9 for the exact solution of the discretized system (——) and the nonbaseband analytical CMS residual flexibility method (- - - -).

C. Experimentally Based Nonbaseband CMS Method Using Residual Flexibility and Residual Inertance Matrices Only

The experimentally based nonbaseband CMS method was conducted using only the residual flexibility of the high-frequency omitted modes and the residual inertance of the low-frequency omitted modes. This was done to show that the nonbaseband method can be applied using data available from existing modal analysis programs. Most existing modal analysis programs allow for the use of residual flexibilities and residual inertances in the curve-fitting process. Using the nonbaseband experimentally based CMS method, these curve fits can be represented exactly in matrix form, provided the necessary driving point frequency-response functions are measured. In this case, $R^S_{aa} = R^C_{aa} = R^G_{aa} = R^H_{aa} = 0$, and as a consequence, $M^u_{\text{comp}} = C^u_{\text{comp}} = K^l_{\text{comp}} = C^l_{\text{comp}} = 0$. The nonbaseband residual flexibility method, however, is unchanged.

The exact residual flexibility of the high-frequency omitted modes and the exact residual inertance of the low-frequency omitted modes were used. The predicted driving point frequency-response function at point 9 and the exact solution are shown in Fig. 5. The coupled results in this case are reasonably good, except for the frequencies of some of the modes. The errors in these frequencies, however, are only −4% (1345 vs 1394 Hz), 3% (3018 vs 2942 Hz), and 11% (4393 vs 3950 Hz) for the first, third, and fourth modes, respectively. This method does not require the optimization of any approximate residual functions and, thus, needs minimal effort. However, the tradeoff is reduced accuracy.

D. Experimentally Based Nonbaseband CMS Method Using Approximate Residual Functions and Model Refinement

The experimentally based nonbaseband CMS method was conducted using approximate residual functions and model refinement.

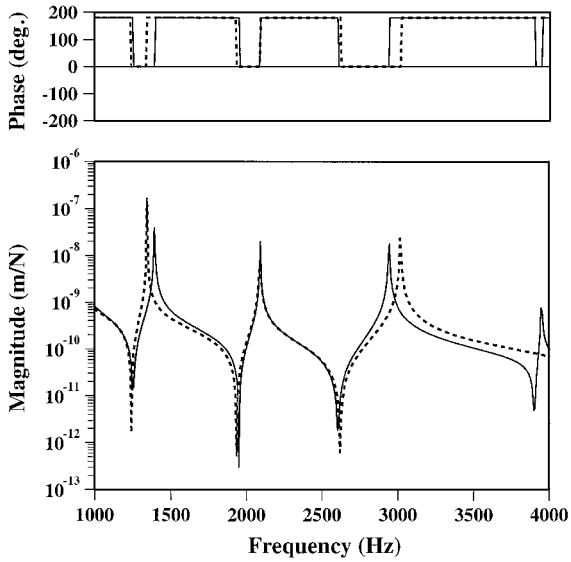

Fig. 5 Driving point frequency-response function at point 9 for the exact solution of the discretized system (——) and the nonbaseband experimentally based CMS method using exact residual flexibility and inertance matrices only (- - - -).

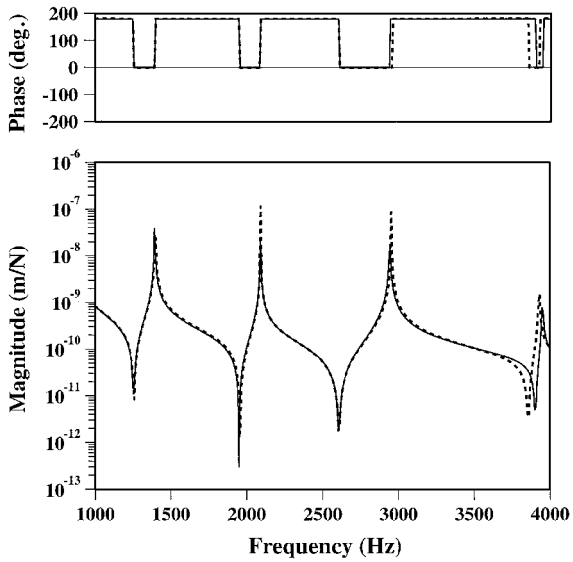

Fig. 6 Driving point frequency-response function at point 9 for the exact solution of the discretized system (——) and the nonbaseband experimentally based CMS method using approximate residual functions and model refinement (- - - -).

The exact residual flexibility of the upper omitted modes and the exact residual inertance of the lower omitted modes were used. Because damping is neglected, $c = \bar{c} = 0$. The two remaining parameters m and $\bar{k}$ were determined using the optimization procedure. Optimization was conducted, and the resulting residual matrices were calculated according to Table 1. The computational modes were determined and were put into the nonbaseband residual flexibility form. Then, the frequency-response functions corresponding to beam 2 were evaluated by comparing the exact results to those determined from the CMS representation. The low-frequency behavior was accurately represented, and so no updating of the low-frequency computational modes was required. The high-frequency behavior was not as accurately represented; therefore, the high-frequency computational modes were mass updated. Proportional mass updating was used as described in Sec. V.C. The updated representation was transformed to the Craig–Bampton form and assembled into the global system matrices. Then the eigenvalues and eigenvectors are determined. The predicted driving point frequency-response function at point 9 and the exact solution are shown in Fig. 6. The coupled results using approximate residual functions and model refinement are seen to be highly accurate in the frequency region of interest.

VII. Conclusion

Three new component mode synthesis methods were developed for application to proportionally damped systems and nonbaseband frequency regions of interest. The methods utilize a modified dynamic reduction method that produces constraint modes at the upper and lower frequency limits of the region of interest. Two analytical methods were presented. The first is based on the Craig–Bampton constraint modes method. This method can be implemented directly in commercial FEA programs and will allow accurate CMS representations to be determined for specific frequency regions of interest. The second analytical method uses a residual flexibility formulation and is the basis for the new experimentally based method. The experimentally based method uses a Maclaurin series expansion to represent the residual effects of the omitted modes. Both low-frequency and high-frequency computational modes are produced. The low-frequency computational modes compensate for the omitted low-frequency modes. The high-frequency computational modes compensate for the omitted high-frequency modes. Excellent results were obtained for the analytical simulation of a system of two coupled beams. The reduced substructure matrices are of the same form as those in the Craig–Bampton constraint modes CMS method. Thus, they can be input directly into commercial FEA analysis programs for substructure coupling analysis and for forced response prediction using the method of Morgan et al.[10] The experimental implementation may be done using the residual flexibility and inertance matrices only, as calculated from existing modal analysis programs, or using approximate residual functions as presented. If approximate residual functions are used, optimization must be performed to determine the parameter values. Further effort is needed to streamline this optimization process, especially in the cases where there are three or more optimization parameters. Also, damping effects are usually difficult to accurately estimate. Alternative methods for their determination may be required. Finally, rotational DOF, in general, will need to be measured and excited to obtain accurate test-derived models. Therefore, both rotational accelerometers and torsional excitation devices will need to be developed.

Acknowledgment

The first author gratefully acknowledges the support by General Motors Corporation under a research fellowship.

References

[1] Morgan, J. A., Pierre, C., and Hulbert, G. M., "Calculation of Component Mode Synthesis Matrices from Measured Frequency Response Functions Part I: Theory," *Journal of Vibration and Acoustics*, Vol. 120, No. 2, 1998, pp. 503–508.

[2] Morgan, J. A., Pierre, C., and Hulbert, G. M., "Calculation of Component Mode Synthesis Matrices from Measured Frequency Response Functions Part II: Application," *Journal of Vibration and Acoustics*, Vol. 120, No. 2, 1998, pp. 509–516.

[3] Craig, R. R., Jr., and Bampton, M. C. C., "Coupling of Substructures for Dynamic Analyses," *AIAA Journal*, Vol. 6, No. 7, 1968, pp. 1313–1319.

[4] Shyu, W.-H., Ma, Z.-D., and Hulbert, G. M., "A New Component Mode Synthesis Method: Quasi-Static Mode Compensation," *Finite Elements in Analysis and Design*, Vol. 24, No. 4, 1997, pp. 271–281.

[5] Kammer, D. C., and Baker, M., "Comparison of the Craig–Bampton and Residual Flexibility Methods of Substructure Representation," *Journal of Aircraft*, Vol. 24, No. 4, 1987, pp. 262–267.

[6] Spanos, P. D., and Majed, A., "A Residual Flexibility Approach for Decoupled Analysis of Systems of Combined Components," *Journal of Vibration and Acoustics*, Vol. 118, No. 4, 1996, pp. 682–686.

[7] Majed, A., and Spanos, P. D., "Nonlinear Dynamics of Structures via Residual Flexibility of Components," *Journal of Aerospace Engineering*, Vol. 10, No. 4, 1997, pp. 173–178.

[8] Rubin, S., "Improved Component-Mode Representation for Structural Dynamic Analysis," *AIAA Journal*, Vol. 13, No. 8, 1975, pp. 995–1006.

[9] Strang, W. G., and Fix, G. J., *An Analysis of the Finite Element Method*, Prentice–Hall, Upper Saddle River, NJ, 1973, p. 58.

[10] Morgan, J. A., Pierre, C., and Hulbert, G. M., "Forced Response of Coupled Substructures Using Experimentally Based Component Mode Synthesis," *AIAA Journal*, Vol. 35, No. 2, 1997, pp. 334–339.

A. Berman
Associate Editor